Thermographic reconstruction of heat load on the first wall of Wendelstein 7-X due to ECRH shine through power

Y. Corre[a], J. Gaspar[b], S. Marsen[c], D. Moseev[c], T. Stange[c], J. Boscary[d], P. Drewelow[c], Y. Gao[c], M. Jakubowski[c], J. Hillairet[a], H.P. Laqua[c], C. Lechte[e], V. Moncada[a], H. Niemann[c], M. Preynas[f], A. Puig Sitjes[c] and W7-X Team

[a] *CEA, IRFM, F-13108 Saint-Paul-lez-Durance, France.*
[b] *Aix-Marseille Université, CNRS, IUSTI UMR 7343, 13013 Marseille, France*
[c] *Max-Planck-Institut für Plasmaphysik, Teilinstitut Greifswald, Wendelsteinstraße 1, 17491 Greifswald, Germany*
[d] *Max-Planck-Institut für Plasmaphysik, Boltzmannstraße 1, 85748 Garching, Germany*
[e] *Institute for Interfacial Process Engineering & Plasma Technology, University of Stuttgart, Germany*
[f] *ITER Organization, Route de Vinon-sur-Verdon, CS 90 046, 13067 St. Paul Lez Durance Cedex, France*

Abstract

Electron cyclotron resonance heating (ECRH) is a powerful and flexible plasma heating technique that serves as the main heating at Wendelstein 7-X and will be used at ITER for start-up, heating, current drive and mitigation of the plasma instabilities. In case of poor or degraded absorption of microwaves, which is expected in O2-mode heating scenario, a significant part of the beam hits directly the wall leading to local overheating and potential damages. The ECRH shine through power is mostly reflected on the targets, only a small fraction being really absorbed through ohmic losses (typically 3% for graphite at 140 GHz). The ohmic losses not only depend on material properties and frequency, but also on polarization of the wave and angle of incidence. The paper presents the thermographic analysis of ECRH experiments at Wendelstein 7-X, including heat load and temperature simulations of the first wall due to ECRH shine through. Two O-mode ECRH experiments with both high temperature rise of the first wall and different angle of incidence of the beam regarding the wall surface are depicted. One experiment has 775 kW power modulation (5 Hz) with mixed polarization (45% O-mode, 55% X-mode) and EC beam angle almost normal to the first wall. The second one has 550 kW steady EC power with O-mode polarization, shallow beam angle and increased power absorption with the material. It is shown that IR thermography is a useful tool to measure shine through power and protect wall components.

Keywords: Electron Cyclotron Resonance Heating, infrared thermography, heat flux calculation
Corresponding author address: CEA, IRFM, F-13108 Saint-Paul-lez-Durance, France.
Corresponding author e-mail: yann.corre@cea.fr

1. Introduction

Wendelstein 7-X (W7-X) is an optimized stellarator with a strong variation of the plasma cross-section from triangular to kidney shape and back, which is repeated in a fivefold toroidal magnetic field symmetry. The device has been designed to operate steady state at a standard magnetic field of B = 2.5 T. Electron cyclotron resonance heating (ECRH) at the second harmonic cyclotron frequency is the main heating technique at W7-X, it is capable of providing up to 7.5 MW of microwave power at 140 GHz (for at least 30 min). A detailed description of the ECRH plant is given in [1]. The ECRH plant has ten gyrotrons that inject microwaves in two out of five modules of the stellarator. Two polarizers per gyrotron in the transmission line allow launching ordinary polarized (O-mode), extraordinary polarized (X-mode), or composition of modes leading to mixed-polarized microwaves into the plasma [2]. Ten 2D steerable microwave launchers in the bean-shaped plasma cross-sections, located in modules 1 and 5, allow a wide range of ECRH and current drive scenarios. Handling such a highly localized heating source requires an extensive set of safety diagnostics [3,4,5]. Infrared (IR) thermography is one of them [6]. It allows observations of thermal footprints from unabsorbed microwave radiation on the graphite tiles of the heat shield that protects the vacuum vessel [7]. Figure 1 shows effect of the ECRH beam on the graphite tile of the first wall as measured with the IR thermography system during the empty torus experiment (without plasma) designed to measure the ohmic absorption.

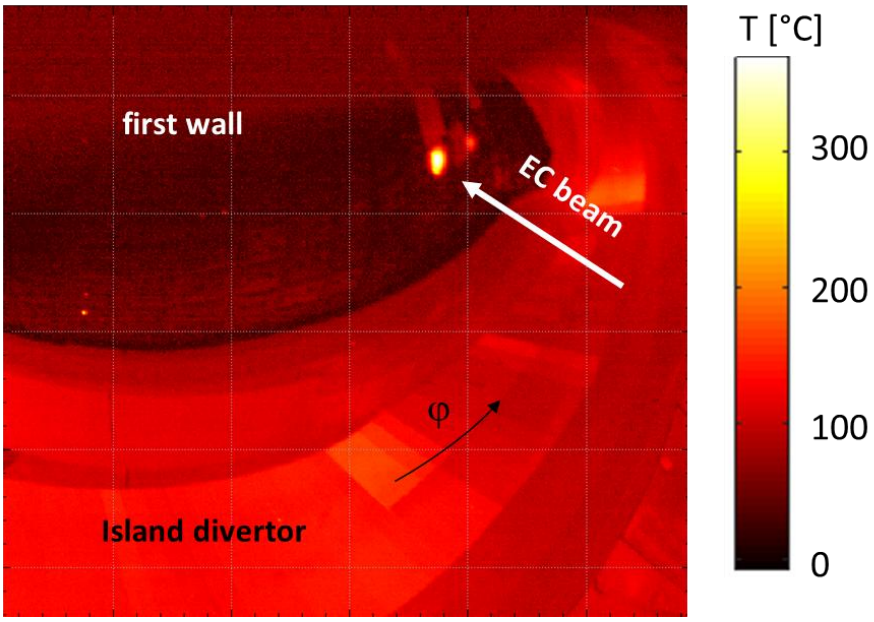


Figure 1: In-vessel view of the infrared thermography system in module 5 of the W7-X stellarator (experiment numbers #20171121.13). The yellow shade shows one of the several ECRH beams launched from the low-field side. In case of no plasma or insufficient plasma absorption the beam hits the first wall, leading to a hot spot on the graphite tiles.

ECRH can be used for wall conditioning, plasma start-up to ionize the neutral gas, heating to bring bulk plasma to temperature and density conditions required for fusion reactions, current drive to sustain long-duration experiment and also in specific places for minimizing the build-up of plasma instabilities to provide improved confinement. The ECRH beam size is narrow (few cm) and has, consequently, a high power density with hundreds of MW□m^{-2} in the center of the beam. Typically, the second harmonic extraordinary mode (X2) is used for plasma heating with more than 99 % absorption for usual plasma parameters [1], but a large power fraction can hit the inner wall especially during plasma start-up which can last several tens of ms or during the second harmonic ordinary mode (O2) which is characterized by lower first-pass absorption (30-70%) compared to X2-mode. The ECRH wave absorption and shine through power are computed with the ray-tracing code TRAVIS [8]. The input beam, absorption zone and shine through power computed for O2 mode polarization are shown in figure 2.

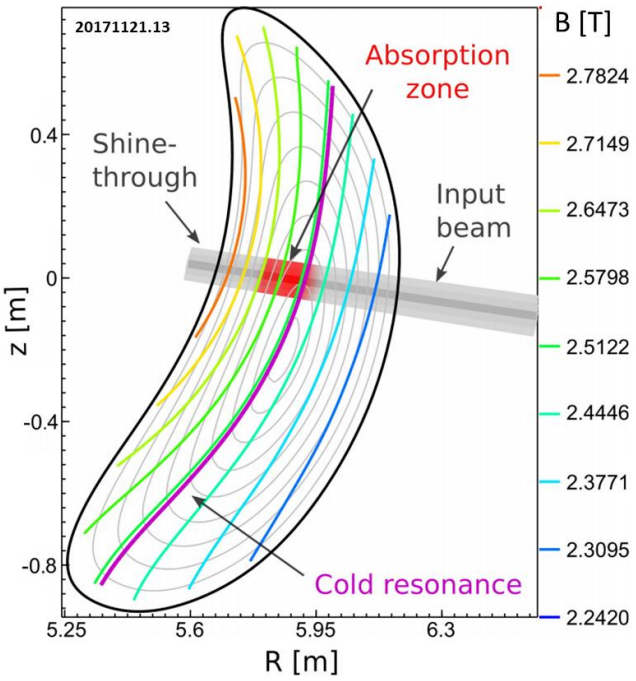


Figure 2: Modelling of the ECRH absorption and shine through power during O2-mode scenario. ECRH ray trajectories are plotted in the RZ-plane for A1 equatorial beam. Magnetic surfaces and B-isolines are also plotted (magenta at $\omega = 2\omega_{ce}$).

How much of the ECRH shine through power is absorbed by the graphite tiles can be calculated by use of a theoretically or experimentally determined absorption coefficient. However, contradictory results were achieved [5] in early shine through and stray radiation measurements performed during the first operational phase of W7-X [9] (OP1.1 including 5 uncooled poloidal

graphite limiters, first wall only partially covers with graphite tiles). Here, heating of the first wall monitored by the thermographic IR systems was reported during ECRH plasma experiments with a duration of only up to 300 ms. Although the accuracy of the power calibration during the start of the gyrotron is questionable due to a frequency shift of typically 200 MHz in the first 300 ms [1]. For this reason, a more detailed investigation of the first wall absorption during quasi steady state ECRH operation is advisable. Furthermore, the fraction of the microwave power absorbed by the inner wall depends on the material properties, beam angle and polarization of the EC wave. In this paper, we present the thermographic analysis of ECRH shine-through experiments at various incident angles. The analysis allows inferring of the microwave absorption coefficients of the graphite armor for different beam angles and polarizations. Presented results are important for other machines, including ITER, since they simultaneously validate the methodology of thermography, confirm that there is a solid understanding of the observations, and provide independent benchmark of properties of materials exposed to high-power microwaves and plasmas.

The paper is structured as follows. Section 2 introduces the physical background and modelling tools: ECRH heat flux, microwave absorption coefficient and heat diffusion through the inner wall. The experimental setup is described in Section 3. Microwave EC experiment performed in the empty vessel, i.e. in the absence of plasma, is presented in Section 4. ECRH shine through experiments are reported in Section 5 for normal and shallow angles on the inner wall. Section 6 concludes the paper.

2. Physical background and modelling

2.1) Microwave absorption coefficient

The absorption of the tile in the microwave region depends on structural properties, morphology of the material surface as well as the incident beam angle and polarization of the beam. Laboratory studies of the absorption losses of different materials at 140 GHz have been performed using a three-mirror resonator technique [10]. These data were used to design the mirrors and cooling system in the transmission system [1]. For perfectly plane materials the absorption of the microwave can be expressed as a function of the angle of incidence (θ, which is defined here as the angle between the propagation axis and the normal vector on the material surface) and the polarization of the beam parallel (E-plane) or perpendicular (H-plane) to the plane of incidence [11]:

$$\eta_{//} = \left(\frac{4}{\mathrm{Cos}\,\theta}\right)\frac{R_S}{Z_0},\ \eta_{\perp} = (4\cdot \mathrm{Cos}\,\theta)\frac{R_S}{Z_0} \quad (1)$$

where Z_0 is the impedance of vacuum (376.73 Ω). R_s is the surface resistance of the material:

$$R_s = \sqrt{R_e \cdot \pi \cdot \upsilon \cdot \mu_0} \qquad (2)$$

where υ is the frequency of the wave. At room temperature, the electrical resistivity are R_e= 11 μΩ.m and R_e= 13 μΩ.m for the two kinds of graphite used on the first wall of W7X (Schunk FP2590 and SGL R6510 manufacturers located in module 5 and 1 respectively). The electrical resistivity decreases with temperature, at 500°C we get R_e= 6.9 μΩ.m and R_e= 8.2 μΩ.m (FP2590 and SGL R6510). The parallel and perpendicular absorption coefficients are plotted as function of the incident angle in figure 3 assuming electrical resistivity R_e= 11 μΩ.m (taken from Schunk FP2590 graphite data library at room temperature).

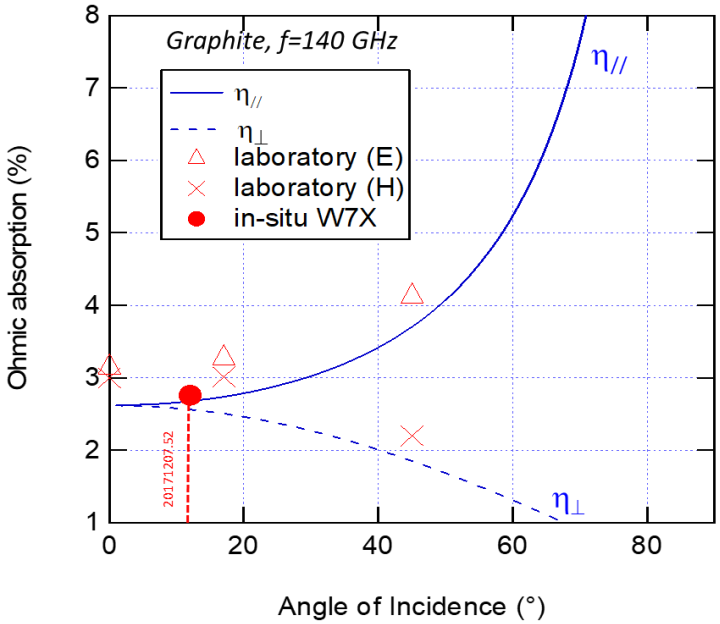


Figure 3: Measured (red symbols) and calculated (blue lines) absorption in graphite (assuming R_e= 11 μΩ.m at room temperature) as a function of the incidence angle for H-plane (dashed line) and E-plane polarization (solid line). Red filled circle is the experimental point obtained in-situ with temperature variation. Red crosses and triangles are laboratory measurements performed at room temperature (tile TH-Z773).

At normal incidence (θ=0°), the absorption coefficient does not depend on the polarization of the beam, it is found to be 2.85% and 2.6% for both materials, R6510 and FP2590 respectively, at room temperature. At higher incidence angle, the polarization of the beam becomes more and more influent. The absorption coefficient increases or falls as the angle of incidence increases, when the electric field is parallel or perpendicular to the plane of incidence, respectively. However, higher angles of incidence correspond to more and more elliptically polarized beams for pure X2- or O2-mode heating, so that even for the high incidence angle, the averaged value is

expected to be lower than expected in figure 3. On top of that, surface effects playing a significant role must be considered (in particular surface roughness).

Two separate measurements (in-situ/laboratory) have therefore been performed to get a more accurate estimation of the absorption coefficient within the W7-X graphite tiles. The first measurement has been performed in 2017 with the tile installed in the machine and 480 kW input power (empty torus experiment depicted in section 4, see red full point in figure 3). The second measurement has been performed in 2020 after removal of the tiles that have been exposed to ECRH beams from the machine (see figure 3, empty triangles and crosses). The losses were measured in a three-mirror Gaussian resonator [12] on three different tiles from W7X corresponding to the three different experiments analyzed in this paper (section 3.2, table 2). Two spherical mirrors form the two-mirror resonator for the fundamental Gaussian mode at 140 GHz. The resonance curve is measured with a vector network analyzer using small coupling holes in the mirror centers for receiver and transmitter. The resolving power of the resonator (quality factor Q2) is calculated. Then, the configuration is changed to the three-mirror setup to overcome additional losses due to diffraction, with the surface under test as the third mirror with incidence angle 17°. The resonator is now folded at 34° but its total length stays the same. The quality factor Q3 is measured and the additional losses introduced by the third surface in the resonator can be calculated from Q2 and Q3. This procedure is repeated for the other polarization and for 45° in case of the back side of TH-Z773. Results are summarized in table 1.

Tile N° (material) / experiment	angle °	plane	Measured loss [%]	Calc. loss [%] (⊥)
TH-Z773 (schunk)/ 20171207.54	45	E	4.12	2.91
	45	H	2.21	3.13
	17	E	3.26	3.12
	17	H	3.01	3.15
In-situ measurement	*12*	*circular*	*2.76*	*2.76*
TH-Z782 (SGL) / 20171121.013	17	E	3.45	3.13
	17	H	3.06	2.87
TH-Z223 (SGL) / 20181009.41	17	E	3.1	3.14
	17	H	3.24	2.87

Table 1: Ohmic absorption (losses %) measured in laboratory (140 GHz ECRH source) for different incidence angle and beam polarization. The power losses at normal incidence (⊥) are derived from equation (1). In-situ measurement is given in italic (empty torus experiment).

Experimental data obtained in laboratory with the three-mirror Gaussian resonator technique are slightly higher than theoretical ones, which is possibly due to surface morphology (structure and roughness). The measurement performed in W7X (in-situ) is slightly lower (2.76%) than

laboratory measurement (ranged from 2.91% to 3.15%). This discrepancy is mainly due to temperature effect because laboratory measurement has been performed at room temperature ~22°C while empty torus experiment had significant temperature increase of the tile from 50°C up to 320°C (480 kW input power during 0.5s). Electrical resistivity is expected to decrease when temperature increases, which is consistent with the experimental observation and equation 1 (power loss being proportional to electrical resistivity). However, the discrepancy between two measurements is tiny, maximum value is 0.4% in absolute and also not so far from theoretical expectation (2.6% assuming R_e= 11 μΩ.m). Furthermore, the differences between the two kinds of graphite (shunk versus SGL) are very tiny: ≤10% in relative. This gives the level of confidence for the shine through power analysis performed in this paper (section 4).

The skin depth, the distance perpendicular to the interface in which the field interior to the conductor drops by factor e, is given by [11]:

$$\delta = \sqrt{\frac{R_e}{\pi \nu \mu_0}} \sim 5\mu m \tag{3}$$

In graphite, the electromagnetic field at 140GHz drops off within a very small distance, typically 5 μm, which is pretty similar to surface roughness. As a consequence, the thermal modelling will be perform assuming surface load only (see section 2.3). To prevent any overheating of the heat shield opposite to the ECRH-launchers the graphite tiles can be coated with tungsten [13]. In this case the absorption coefficient is only $\eta_W \leq 0.3\%$ [10], almost one order of magnitude lower than graphite, so that even the absorption of the full power ECRH beam is below the heat load limit of the particular tiles of the ECRH heat shield.

2.2) EC beam size and heat flux density

In the plane perpendicular to the propagation of the microwave, the power distribution of the EC beam is supposed to be Gaussian:

$$q_{EC}(x,y) = q_{EC}(0).exp^{-\frac{2x^2}{w_x^2}-\frac{2y^2}{w_y^2}} \tag{4}$$

where $q_{EC}(0)$ is the peak heat flux density, x and y are spatial coordinates in the plane perpendicular to the propagation axis, w_x and w_y represents the width of the beam in the x and y direction. The beam size is the distance from the propagation axis at which the power has fallen to $\frac{1}{e^2} \sim 13\%$ of its on-axis value, $q_{EC}(0)$. On the propagation axis, the peak heat flux density, $q_{EC}(0)$, is simply derived from the integral of the Gaussian surface distribution in the plane perpendicular to the propagation axis as given in [5]:

$$q_{EC}(0) = \frac{P_{EC}}{\int_{-\infty}^{+\infty} exp^{-\frac{2x^2}{w_x^2}-\frac{2y^2}{w_y^2}} dx.dy} = \frac{2.P_{EC}}{\pi.w_x w_y} \tag{5}$$

where P_{EC} [W] is the total propagation power. The spatial distribution of the heat flux density delivered by the ECRH launcher is presented in figure 4 for different beam sizes $w = 30, 40, 50\ mm$ and 1MW power injected (P_{EC}) before plasma absorption.

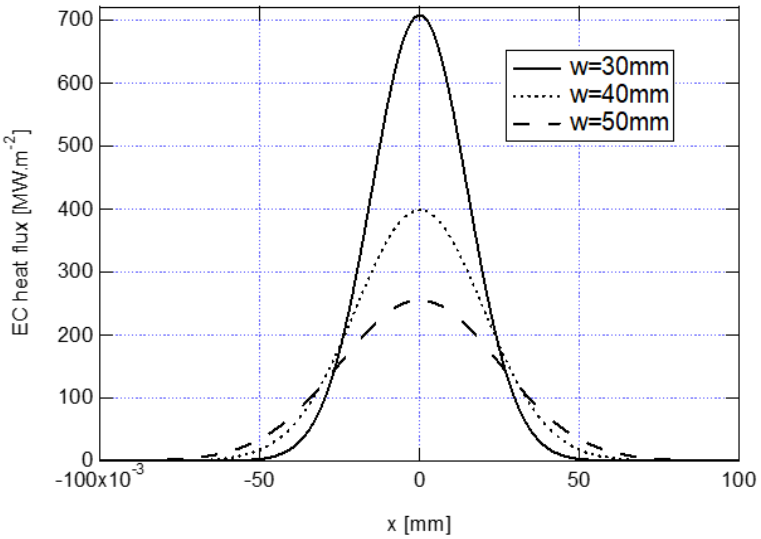


Figure 4: Simulated EC heat flux distribution assuming a beam size of 30, 40, 50 mm and 1MW power injected.

Assuming a cylindrical symmetry of the beam (w_x=w_y=w), a gyrotron delivering 1MW with EC beam size of 30 mm would have, according to equation (5), 700 $MW.m^{-2}$ heat flux density on the propagation axis. After the first path absorption, only a small part (few % for graphite as shown in figure 3 and even less for metallic reflectors) of the transmitted ECRH power is finally absorbed by the tile located in front of the steering mirror. ECRH experiment with empty plasma vessel has been performed on purpose in order to derive the experimental beam size and absorption coefficient on graphite tiles (η_C) based on the analysis of the IR thermography data (see section 3).

2.3) Description of the tile and thermal modelling

One part of the first wall is covered by graphite tiles which are clamped with TZM screws on a 9 mm thick copper-chrome-zirconium (CuCrZr) heat sink designed for active cooling during steady state plasma and continuous-wave (cw) operation, as planed during the next operation phase (referred to OP2) [14]. The graphite tiles are currently uncooled (there was no water flows in the heat sink during OP1) and have been shaped on plasma facing surface in order to prevent the leading edges with quasi-normal incidence of the parallel plasma heat flux. A typical tile geometry is presented in figure 5-a: each tile includes five facets: left, right, top, down and central one with diamond-shape. The length is 99 mm, width 89 mm and thickness is 10 mm at the central top surface. The thermal contact between graphite and structure plate is provided by a

1mm SIGRAFLEX® layer inserted at the interface. The backside of the structure plate is supposed to be adiabatic (no contact with other components).

Temperature distribution on the graphite tiles is modelled in a transient way with a finite element method (FEM), CAST3M code [15]. The heat flux is assumed to have Gaussian shape as expected by the ECRH wave propagation theory (equation 4) and the shape of the tile is supposed to be rectangular. Surface shaping can be neglected here because, contrary to plasma heat flux in the scrape-off layer (SOL) which can reach the leading edge of the tiles, the ECRH beam hits the wall with low angle of incidence (regarding to the normal vector on the material surface). To take into account for the finite size of the component (both parts: tile and structure plate) and shape of the heat flux distribution profile, the modelling of the mesh is 2D. The skin depth of the microwave beam being small, few micrometers (equation 3), the heat flux density (q_n) is imposed on the flat top part of the tile, as depicted in figure 5-b).

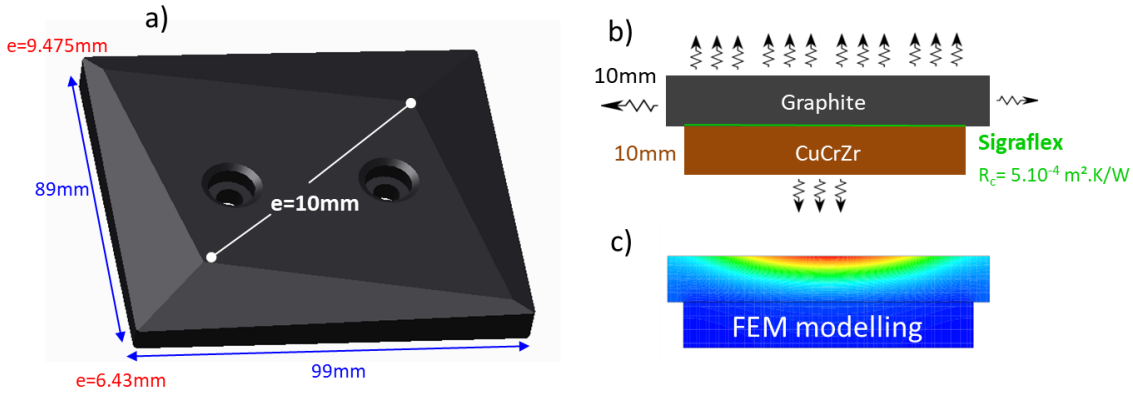


Figure 5: (a) CAD view of the graphite tile. 2D cross section of the assembly: (b) schematic picture of the assembly and (c) thermal modelling performed by CASTEM.

The thermal properties of each material (graphite, CuCrZr) depend on temperature. The graphite material is isotropic (thermal conductivity K ~ 100 $W \cdot m^{-1} \cdot K^{-1}$ and ~ 50 $W \cdot m^{-1}. K^{-1}$ at T=ambient and T = 1000 °C) with open porosity of 10%. The TZM screws have been designed to create a contact pressure of 0.25 MPa (at room temperature) to ensure thermal contact of $5 \times 10^{-4}\ m^2.K/W$ at the interface between the graphite tile with the CuCrZr heat sink. However mechanical strength at the clamping screw may vary from one tile to another one in the overall device as function of tightening, mechanical deformation and strength occurring after successive plasma operation and the thermal contact could vary slightly from the original value. The radiative exchanges between the plasma-facing surface, the lateral faces and the environment are taken into account. The temperature of the radiative environment is assumed to be 30 °C, which is the typical temperature of the machine when plasma facing components (PFCs) are completely cooled. According to the time duration between two consecutive pulses and the energy injected

during the previous pulse, some parts of the machine can be locally hotter when the pulse starts. The initial temperature of the inner tiles targeted with the EC beam were typically between 50°C and 70°C for the series of pulse analyzed in this paper. Some of the divertor tiles were above 100°C because of the energy accumulated during the previous pulses. The heat thermal diffusion time in the graphite layer is computed as follows:

$$\tau_{diff} = \frac{e^2}{a} \sim 2s \quad (6)$$

for thickness e=1cm and thermal diffusivity of graphite a = 5.10^{-5} $m^2.s^{-1}$. For heating duration below such value ($\tau_{heating} \leq \tau_{diff}$), thus for short experiment such as ECRH start-up or ECRH shot in empty torus (see section 3.2), the thermal modelling of the temperature rise and the heat flux calculation do not depend on R_c. For longer heating duration ($\tau_{heating} > \tau_{diff}$) or during the cooling of the tile, both phenomenon thermal contact (R_c) and heat diffusion through the CuCrZr structure become important. To avoid any damages of the tile and their support structure, the surface temperature of the tiles should be maintained below 1200°C. This has been determined considering the copper in the support structure which is expected to have thermo-mechanical degradation above 450°C.

3. IR thermography during ECRH experiments

3.1) Experimental set-up: IR cameras

From the start-up of the reactor in 2016, several IR systems have been deployed, step by step accordingly to the W7-X completion, in order to protect the plasma facing components (divertor target, baffle, heat shield and wall panels) during plasma experiments. In OP1.2 experiments, running with uncooled plasma facing components, 1 prototype IR endoscope with a field of view of 115° horizontally and 60° vertically and 9 basic IR systems based on immersion tubes having a field of view of 115° horizontally and 100° vertically have been deployed in the top of the device. The IR cameras used in the immersion tubes have 1024 × 768 pixels, with a pixel size of 17 × 17 μm working in the spectral range from 8 to 14 μm (LWIR) with a maximum frame rate of 120 Hz while the IR camera used in the endoscope is working in the spectral range from 2 to 5.7 μm. These two IR systems have been used to develop and test the IR real-time protection [16] and hot spot detection algorithms [17] foreseen in preparation of OP2 with actively cooled components and long-duration capabilities.

The accuracy of the IR thermography measurement usually suffers from emissivity uncertainties of the material. In W7X surface temperatures are obtained with in-situ black-body calibration assuming surface emissivity is equal to 0.82 as expected for the original surface of graphite. Laboratory measurements performed on sample taken from W7X has evidenced variation of emissivity as function of plasma exposure, from 0.82 (original surface) up to 0.95 for rough

surfaces (close to blackbody) [18]. On the inner side of the first wall, we don't expect any modification due to plasma erosion because the last closed flux surface is few cm away because of five poloidal graphite limiters mounted on the inboard side of the vessel. However, wall conditioning such as boronization or powder injection techniques have been routinely performed and could have an impact on the thermo-radiative properties of the surface. The accuracy of the absolute temperature measurement due to emissivity uncertainty has been computed in the temperature range obtained during the W7X ECRH experiments (see Fig. 6) assuming surface emissivity of 0.7 (minimum) and 0.95 (maximum).

$$B(T_{IR}) = \varepsilon_{IR}.B(T_{real}) + (1 - \varepsilon_{IR})\mathrm{B}(T_{amb})$$

Where T_{IR}, T_{true} and T_{amb} are the IR temperature measurement (here assuming $\varepsilon_{IR} = 0.82$), the true temperature of the component and the ambient temperature (T_{amb} = 20°C here). The spectral radiance is given by the Planck's law:

$$\mathrm{B}(\lambda, \mathrm{T}) = \frac{2hc^2}{\lambda^5\left(exp^{\frac{hc}{\lambda kT}} - 1\right)} \quad (7)$$

Where λ is the wavelength (IR filter), h is the Planck constant, k is the Boltzman constant and c is the light celerity.

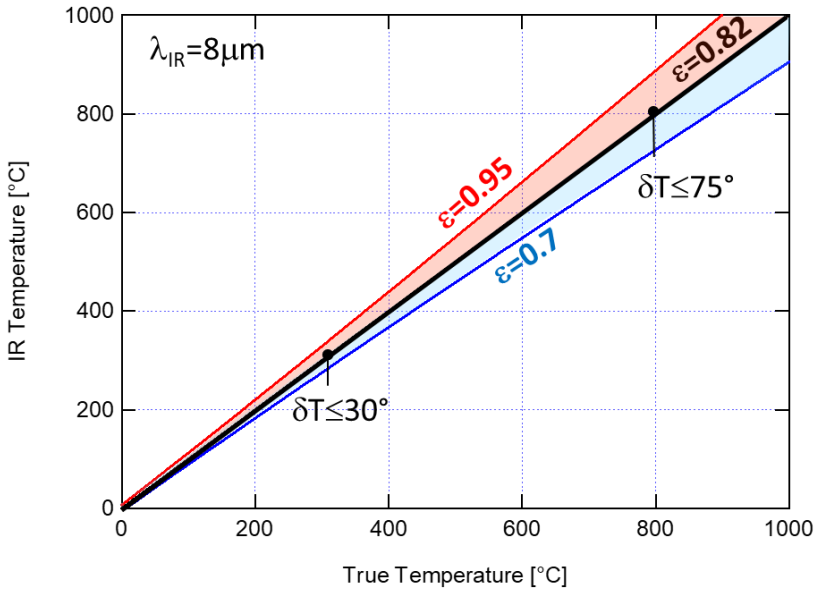


Figure 6: Error bar due to emissivity uncertainties for λ_{IR}=8µm. Lower and higher emissivity lead to under (blue) and over-estimation (red) of the true surface temperature.

The maximum discrepancy between the most extreme values of emissivity (0.7 and 0.95) and the IR one ($\varepsilon_{IR} = 0.82$) are δT= 30°C and 75°C for IR surface temperature of 300°C and 800°C respectively. If true emissivity is 0.7, this means the real surface temperature can be

underestimated by almost 10% if the emissivity is assumed to be 0.82. If true temperature is 0.95, then this means the real surface temperature can be overestimated by almost 10%.

3.2) ECRH experiments performed in W7-X

The 140 GHz ECRH beams are launched from the low-field side into the machine by front steering launchers through equatorial port plugs located in the torus modules N°1 and 5. The movable mirrors enable a poloidal steering range of ±30 degree and a toroidal steering range between -15 and +35 degree [1]. Such flexible launching system enables to operate with the different heating scenarios (mode coupling). For standard magnetic field (B=2.5 T), second harmonic X2- and O2-mode heating are used for low and high density plasma operation, below and above the X2-mode cut-off density of $1.2 \cdot 10^{20}$ m^{-3} respectively [19]. The O2-mode is characterized by lower first-pass absorption (30-70%) compared to X2-mode (>99%) heating scenario. Therefore, a set of metallic reflectors have been installed on the inner wall in order to reflect the transmitted power with an optimum angle to maintain a well-defined second pass absorption in the plasma during O2-mode operation. The setting of the steering mirror or the wave polarization regarding the discharge requirements was not always guaranteed during the first ECRH experiments; it happened accidently that the EC beam was directed toward the graphite instead of metallic tiles during O2-mode heating scenario. In this paper, we propose to investigate two of these experiments which have the benefit of offering high quality IR data (significant temperature rise on highly emissive material) compared to metallic reflector tiles.

The first experiment analyzed has been performed on request to evaluate the microwave absorption (equation 1) by the graphite material with empty vessel (without plasma). Here, a 480 kW ECRH beam was launched centrally on bigger graphite tile (length 111 mm, width 98 mm) with almost normal incidence (see figure 1). Since there is no plasma, there is no absorption at all on the first pass and the power reaching the tile is therefore equal to the input power. The central incidence on the tile allows accurate reconstruction of the beam width as well as accurate thermal modelling. Furthermore, a circular polarization was used to reduce the risk of arcing on the tile or any other inhomogeneity connected to linear polarization. In the second analyzed experiment, a 775 KW ECRH beam was pulsed with a frequency of 5 Hz and a duty of 160 ms to 40 ms on/off. Here, the polarization was a mixture between O2-mode (45%) and X2-mode (55%) achieved with external polarizers (allowing to configure composition of modes) and the beam was directed on graphite tile (usual mirror settings for pure X2-mode scenario) instead of metallic reflector (usual mirror settings for O2-mode scenario). This was leading to a pulsed heat up of the graphite tile by the transmitted O2-mode part (see launching geometry in figure 7-a with almost normal incidence). The third experiment was conducted with an O2-polarized beam with 550 kW power, but wrong beam direction hitting graphite tiles under shallow incidence (figure 7-b).

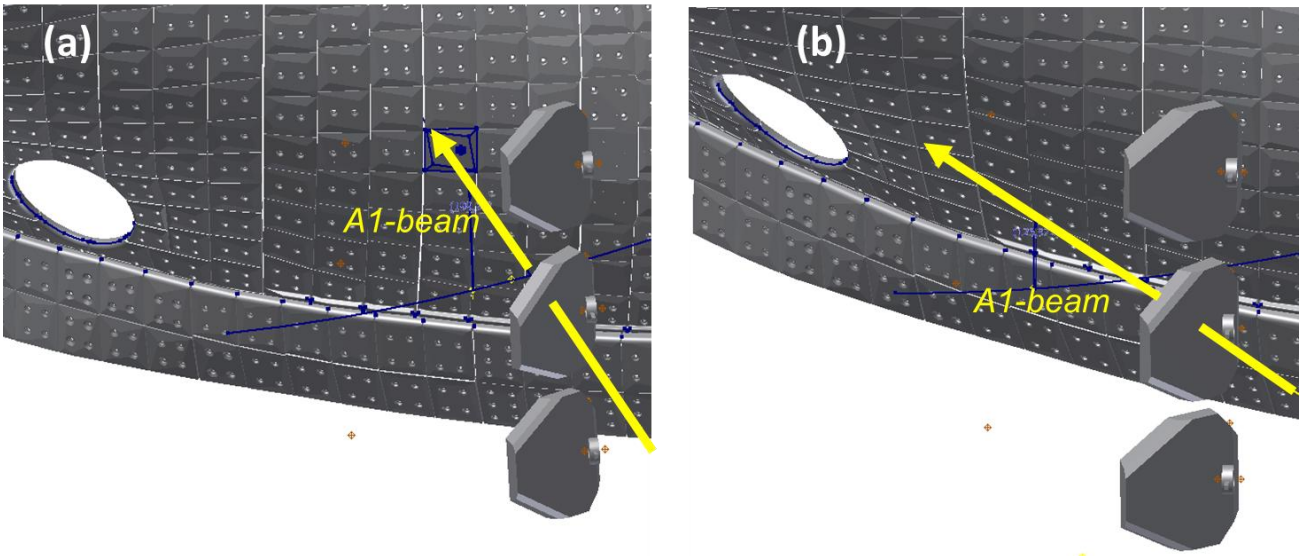


Figure 7: Launch scenario for (a) #20171121.13 with θ=17° (almost perpendicular) and (b) #20181009.41 with θ=58° (shallow angle).
The EC beam and the impacted tile are shown in yellow line and arrow respectively.

The main experimental parameters used in these three experiments are summarized in table 2: Launch scenario (figure 7), tile number, EC beam module, EC beam power, angle of incidence (θ), plasma duration, core plasma density, input power, theoretical shinethrough power computed with TRAVIS ray-tracing code [8], polarization of the EC beam (elliptical), ohmic absorption assuming $\eta_c = 3\%$ at 0° and maximum surface temperature reported by IR thermography on the graphite tile (assuming ε=0.82).

Experiment	20171207.54	20171121.013	20181009.41
Tile	TH-Z773	TH-Z782	TH-Z223
Beam	D5	A1	A1
θ [°]	12	17	58
Duration [s]	0,5	10	8,5
Density [m^{-3}]	0,00	$1.8 \cdot 10^{19}$	$5.5 \cdot 10^{19}$
Input-Power [kW]	**480**	**775**	**551**
Duty		On: 0,16s Off: 0,04s	Cw.
O-mode-part		0,45	1,00
O-Absorption	0,00	0,32	0,29
X-Absorption	0,00	1,00	1,00
Sum Absorption [kW]	0,00	537	160
Shine through [kW]	**480**	**238**	**391**

Polarization ⊥ [%]	Nc.	21	46
Polarization // [%]	Nc.	79	54
Ohmic abs. η_C ⊥		2.87	1.60
Ohmic abs. η_C //		3.14	5.63
Averaged η_C		**3.08**	**3.78**
T_{surf} [°C] maximum	320	880	710

Table 2: Summary of the plasma and technical parameters for the pulses depicted in this paper.

The angle between the ECRH beam with the normal vector of the tile surface (θ) is used to compute the broadening of the beam on the top surface of the tile, which is given by $\frac{1}{\mathrm{Cos}\,\theta}$. For angles below 20°, the geometrical projection remains negligible and the EC beam width can be directly used as input for the thermal modelling (section 2.3). Moving further away from normal incidence, broadening increases and the beam footprint becomes elliptical, $w_x > w_y$ (equation 4), assuming x and y coordinates are horizontal and vertical direction of the tile respectively. As a consequence, the power reaching the tile is spread over the tile surface and the peak heat flux reaching the top surface decreases as function of the broadening of the beam.

3.3) IR data processing and visualization

IR data are displayed and processed using THERMAVIP software [20] developed for real-time and off-line data analysis. THERMAVIP provides data access with wide range of formats, visualization features and many video processing such as temperature profile along polylines, maximum temperature in Region Of Interest (ROI) and image operations (overlap, addition and subtraction). A separate image processing system has been developed with computer-aid-designed (CAD) model and optical distortion model to get spatial calibration of the IR videos [21]. IR data recorded during shinethrough experiments and overlapped with 2D CAD geometry of the inner wall (also called scene model) are displayed in figure 8 for two angles of incidence θ=17° and 58°. The figure shows heating of the island divertor due to heat plasma exhaust and a circular hot spot on the inboard first wall. The hot spot represents the heating of the graphite tile caused by shinethrough power reaching the first wall. For the almost normal incidence angle (a), the ECRH hot spot is localized in the mid-plane, almost in front of the ECRH plugin. For the shallow incident angle (b), the ECRH hot spot is localized below the mid-plane and on the left of the ECRH plugin. The IR measuring system being located on the top of the machine, the inner wall surface shows an inclination regarding the IR line of sight, in particular for the shallow angle. Therefore the pixel size has to be computed locally, for each ECRH hot spot. The pixel

size is determined with the 2D CAD geometry which allows plotting temperature profile across the tile (from one gap between tiles to the opposite one). The uncertainty related to the evaluation of the pixel size and therefore the beam width is at best one IR pixel. The accuracy attributed to the data processing for spatial calibration is set to ±1 pixel.

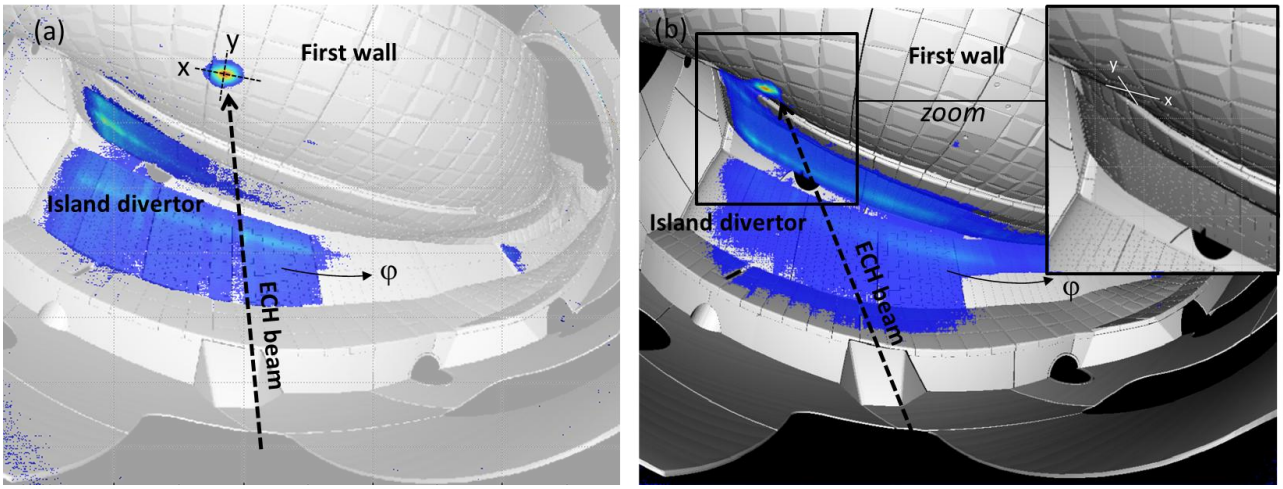


Figure 8: IR data during W7-X ECRH plasma experiment with shinethrough power hitting graphite tiles and CAD geometry of the inner wall in the scene model. (a) #20171121.13 with θ=17° (775 kW modulation 5 Hz, duty cycle) and (b) #20181009.41 with θ=58° (551 KW continuous heating)

4. ECRH beam (480kW) without plasma

By knowing the beam size and peak heat flux from IR data, it is easy to derive the power received by the tile (equation 5). The question is how much of the microwave ECRH power is effectively absorbed by the material? As described in section 2.1, the absorption coefficient varies first and foremost with the incident angle as well as the polarization of the wave. Secondly, it could also depend on the surface (roughness or coatings) of the material which can vary in the plasma environment due to erosion and deposition processes. To resolve this issue, a shot with 480 kW EC power (circular polarization) was launched on request in an empty plasma vessel.

The shot was performed with short duration (0.5 s) to avoid any damage on the tile and with an incidence angle with the wall almost normal (θ=12°) to avoid any influence of the beam broadening. The projection of the ECRH beam on the first wall is therefore almost circular $w_x \approx w_y$. The beam size is derived by IR thermography using spatial calibration as depicted in the previous section. The temperature data are extracted along both, horizontal (x) and vertical (y) direction in the local coordinates of the tile. The spatial resolution is found to be 4.4 mm/pixel and 2.96 mm pixel on the horizontal (x) and vertical direction (y) respectively. The beam size is

derived from a Gaussian fit (equation 4). We found $w_x = 44 \pm 4.5mm$ (see figure 9 – a) and $w_y = 42 \pm 3mm$ on horizontal and vertical profiles respectively. These values are slightly higher than the theoretical beam width expected from the imaging properties of the ECRH launcher ($w_{sim} = 37mm$). However, the discrepancy between IR measurement and numerical calculation is small, about 4 mm and can be attributed to the tile geometry and fitting procedure of the temperature profile on the wings of the Gaussian which is not so smooth because of the gap between tiles. After 0.5 s heating, the surface of the tile reached about 320°C at maximum which is safe for this component (far from technological limit sets to 1200°C). Thermal modelling is then performed in an iterative way: the peak heat flux absorbed by the graphite (q_n) and the thermal resistance (R_c) are adjusted in order to match the experimental data during heating and cooling down phase, respectively. The initial tile temperature is set to T_0 = 50°C as measured with IR data.

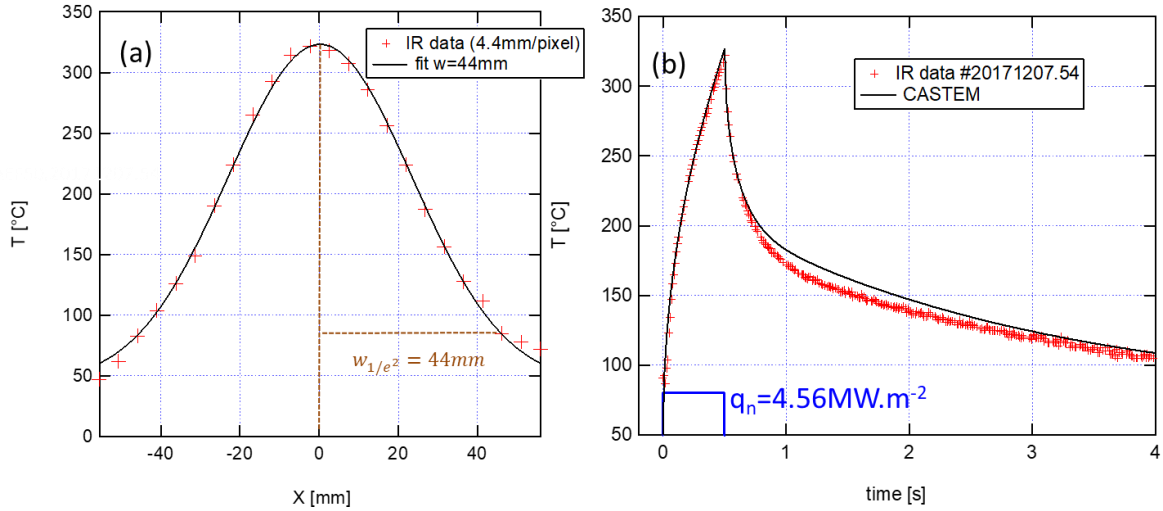


Figure 9: (a) Temperature distribution extracted from IR movie at t=0.5s (at the end of the EC shot). Experimental data are fitted with Gaussian function (equation 4). (b) Maximum temperature on the tile surface, IR measurement (red points) and CASTEM simulation (black line) after iterative loop.

The time evolution of the surface temperature measured by IR thermography system and modelled with CASTEM [15] are presented in figure 9-b (maximum temperature). We found a good match between IR data and modelling with q_n = 4.56 MW.m^{-2} and $R_c = 1.7 \times 10^{-4} m^2 K/W$. The agreement is almost perfect during the heating phase and remains satisfactory during the cooling of the tile, when the heat passes through the graphite tile and diffuses into the CuCrZr heat sink structure located behind the graphite tile. The accuracy of the heat flux calculation depends on several parameters such as the accuracy of the IR temperature measurement, the thermal properties of the material, the beam width (set to ±1pixel here) and the bounding of the

tile on CuCrZr structure (R_c, which is derived in the cooling phase). The error bars due to IR absolute temperature measurement are set to 10% because of the emissivity uncertainties (as shown in section 3.1). The error bars associated to the thermal properties are ignored because the data used are given and certified by the manufacturer. The error bars associated to the bounding of the tile are also ignored here because the heating duration (0.5s) is lower than the heat thermal diffusion time of the tile (2 s as computed in equation 6). The error bars attributed to beam width and emissivity uncertainties are given in table 3, it is less than 1% for the beam width and 10% for the emissivity.

	w-δw=39.5mm	w=44mm	w+δw=48.5mm
q_n (MW.m^{-2})	4.59	4.56	4.53

	ε=0.7	ε=0.82	ε=0.95
q_n (MW.m^{-2})	5.02	4.56	4.25

Table 3: Heat flux required to reach 320°C on top surface after 0.5s heating with different beam widths and different emissivities. The difference gives an estimation of the error bars attributed to the beam width and emissivity.

The ECRH heat flux absorbed by the tile during this experiment is $q_n(0) = 4.56 \pm 0.4 MW.m^{-2}$. This result is then used in the second step to derive the microwave absorption by the graphite, which is defined as:

$$\eta_C = \frac{q_n(0)}{q_{EC}^{trans}(0)} \quad (8)$$

Assuming a beam size of $w_x = 44mm$ and $w_y = 42mm$ as obtained experimentally and 480 kW ECRH input power, we would expect peak heat flux transmitted by the wave $q_{EC}^{trans}(0) = 165\ MW.m^{-2}$ (equation 5). The microwave absorption coefficient by graphite is therefore found to be 2.76% (equation 8) with 10% under and 7% overestimation in case of lower or higher emissivity respectively. The experimental value is coherent with both theoretical values (2.6% for FP2590 as used for the graphite tile in module 5) expected at normal incidence with perfectly plane surface and laboratory measurements (mean value is 3% as depicted in section 2.1).

5. ECRH heating with finite shine through

5.1) 775 kW ECRH modulation (O/X mixture)

A shot with total of 3 MW EC power, spread over 2.2 MW steady state in X-mode and 775 kW modulation with 5 Hz frequency with mixed O/X polarization has been performed to assess

the capabilities of the collective Thomson scattering (CTS) diagnostic for energetic ions. The shot is interesting for several reasons. The first reason is the significant level of power 775 kW (close to maximum) launched by one gyrotron with wrong polarization and the subsequently high temperature of the impacted tile (880°C at the end of the pulse). The question regarding wall protection is what would be the temperature of the CuCrZr structure plate to comply with the technological limit? The second reason is the power modulation leading to successive heating and cooling of the tile which is particularly useful to derive both parameters: peak heat flux (q_n) during heating and thermal resistance (R_c) between tile and heat sink structure during the cooling phase. The last reason is the beam angle which is close to normal (θ=17°) so that absorption coefficient is almost insensitive to the wave polarization (see figure 3).

After 10s heating, the surface of the tile reached about 880°C maximum which is below the temperature limit for graphite (1200°C) and safe for the plasma operation. The size and position of the EC beam are derived from IR thermography using spatial calibration data processing as depicted in the previous section. The temperature data are extracted along both, horizontal (x) and vertical (y) direction in the local coordinates of the tile. The spatial resolution is found to be 1.6mm/pixel and 2.5mm/pixel in the horizontal (x) and vertical (y) directions respectively (see figure 8-a). Figure 10 shows the temperature distribution profiles along x (a) and y (b) coordinates extracted from IR data (red crosses) and obtained after fitting process (black line).

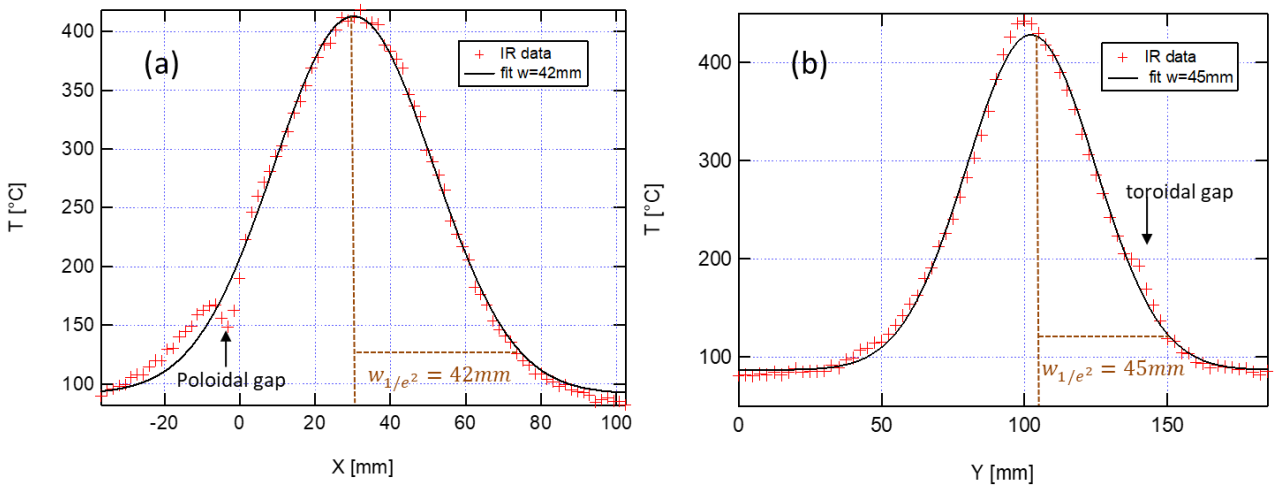


Figure 10: Horizontal (a) and vertical (b) temperature distribution extracted from IR movie at t=2s. Experimental data are fitted with Gaussian function as given in equation 4. The sides of the tile are spotted by the gaps between two neighboring tiles.

The beam size is derived from a Gaussian fit (equation 4). We found $w_x = 42 \pm 1.6mm$ and $w_y = 45 \pm 2.5mm$ on horizontal and vertical profiles respectively. The standard deviation

computed after the fitting process is found to be lower than the pixel size in both directions, horizontal and vertical. The accuracy of the beam width measurement is therefore kept to ±1pixel as explained in section 3.3. The experimental values are slightly higher than expected ($w_x = 37.8\,mm$ and $w_y = 37.5\,mm$) and very close to previous values (empty torus experiment with θ=12°). For this pulse, the angle of the beam with the normal vector with the tile surface was θ=17° and we expect a very small broadening effect during the projection with the tile surface, typically 5%. However, as for the empty torus experiment, the discrepancy between measurement and numerical calculation is small, about 5 mm and can be attributed to the tile geometry and fitting procedure of the temperature profile on the wings of the Gaussian which is not so smooth because of the gap between tiles. The beam size derived from IR data is then used as input for the thermal modelling. The final step aims to fit the experimental maximum temperature time evolution with numerical thermal modelling. This is done in an iterative way adjusting the peak heat flux (q_n) and thermal resistance (R_c) in order to match the experimental data during heating and cooling phase, respectively, up to the end of the pulse (reaching 880°C here). The initial tile temperature is T_0 = 50°C. For each run, or set of input parameters, we compute the root mean square with the IR experimental data (figure 11):

$$\sigma = \sum \frac{\left(T^{IR} - T^{castem}\right)^2}{N} \tag{9}$$

where N is the number of experimental points (from the starting to the end of the ECRH shot).

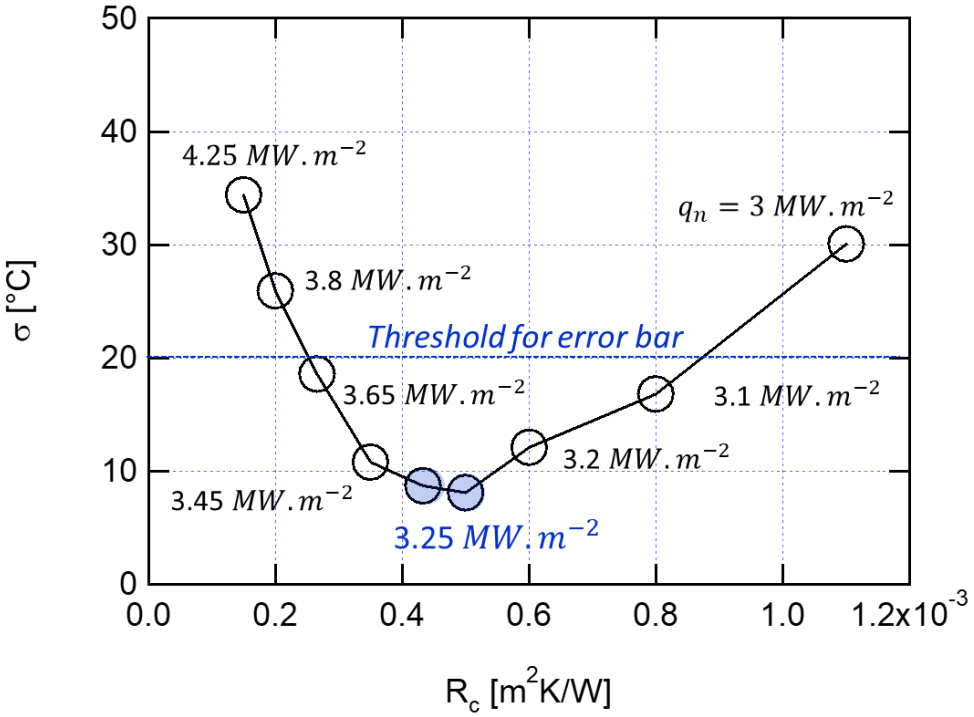


Figure 11: Root means square computed for several runs (CASTEM) plotted as function of the bounding coefficient (Rc). Peak heat flux values are given in the plot.

Its minimum value is σ=8.1° for the full sequence (see fig. 11), which is small compared to the surface temperature up to 880°C at the end of the shot. This can be explained by small discrepancies between experiment and modelling assumptions (rectangular geometry, boundary condition, EC loads and step chronology, which sometimes differ slightly). The minimum value of the root mean square, which corresponds to the best match between IR data and modelling, is found with q_n = 3.25 MW.m^{-2} and $R_c = 5\ 10^{-4} m^2K/W$. Higher and lower R_C value would result in under and overestimation of the heating (ΔT~48°) and cooling phases (ΔT~36°), respectively (figure 12-b). The accuracy of the heat flux calculation can be sorted out from the root mean square distribution using a maximum acceptable value. Fixing an average of 20° discrepancy per data point as a maximum acceptable value, which is quite penalizing, leads to heat flux values in the range of [3.1 – 3.7] MW.m^{-2}. The numerical accuracy would be therefore about 11%. The time evolution of the surface temperature measured by IR thermography system and modelled with CASTEM are presented in figure 12 (maximum temperature).

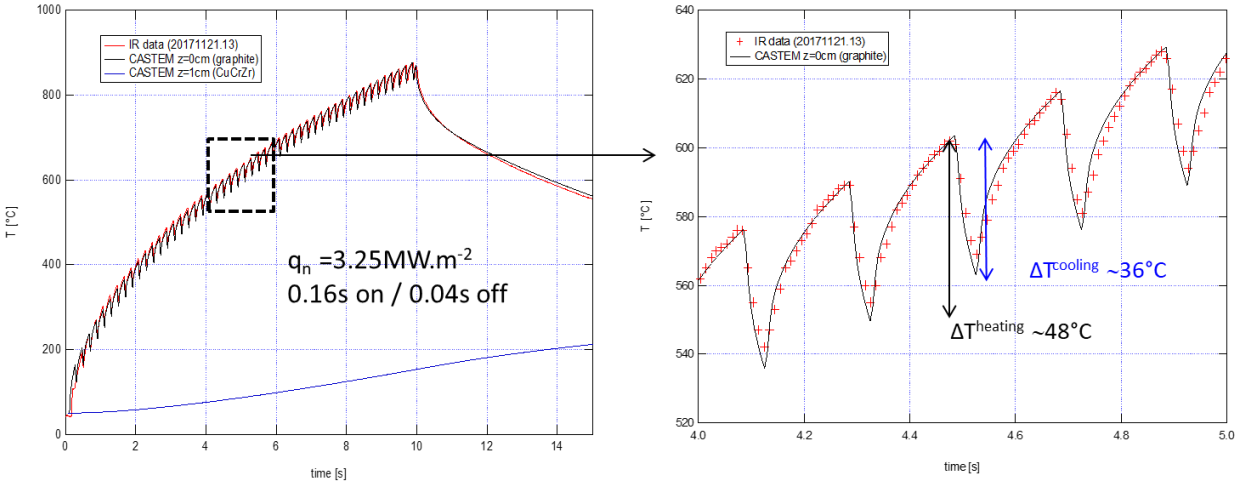


Figure 12: Maximum temperature on tile surface, IR measurement (red points) and CASTEM simulation (black and blue lines on top surface and CuCrZr interface respectively) after iterative loop (a) full pulse and (b) zoom over 5 periods

The thermal resistance derived from this pulse ($R_c = 5\ \times 10^{-4}\ m^2K/W$) is equal to the theoretical value and pretty close to the one derived from the pulse with empty torus ($R_c = 1{,}7\ \times 10^{-4} m^2K/W$). Such discrepancies are small and can be explained with the clamping screw or SIGRAFLEX® layer which could be different from tile to tile all over the in-vessel of the device. However a good agreement is obtained during both heating (ΔT~48°) and cooling

phases (ΔT~36°) of the ECRH pulsation. The temperature calculated at the interface between graphite and CuCrZr heat sink is also shown in figure 12-a (blue line). Five second after the end of the pulse, the CuCrZr heat sink reaches 210°C. The overall cooling of the tile is slow because it is ensured with surface radiation and conduction through the TZM screws. 20s after the end of the pulse, the maximum temperature reported with the modelling at the interface is close to stabilization near 300°C, which is below temperature limit of 450°C and safe for the component.

Using the experimental heat flux and the tile absorption coefficient derived in the previous section (at almost normal incidence), we can now determine the transmitted EC peak heat load (equation 8). Assuming $\eta_C = 3.08\%$ as computed in table 2, one finds peak transmitted power of $q_{EC}^{trans}(0) = 105\ MW.m^{-2}$. Assuming $w_x = 42$ mm and $w_y = 45$ mm beam widths, this represents about 301 kW ECRH shine through power (38% of the total input power including X and O-mode) which is larger than numerical expectation (238 kW, table 2). The discrepancy (20%) is higher than error bars associated to IR measurement (10%) and theoretical calculation (15%). For this particular pulse with O/X polarization mixture, the heating of the tile due to ECRH is larger than expected numerically.

5.2) Steady state (8s) ECRH operation in O-mode with low plasma absorption

A pulse has been performed with 3.5 MW of ECRH in O2-mode scenario in which one gyrotron delivering 550 kW had wrong positioning of the mirror regarding the inner wall (the beam faces the graphite tile instead of the metallic reflector as usually planned during the O2-mode scenario). After 8 s of steady ECRH plasma heating, this leads to significant increase of temperature on the graphite tile, about 710°C. This pulse is also of particular interest because the angle of incidence is higher (θ=53°) compared to the two pulses analyzed before (12° and 17°), so an effect of the polarization of the wave is expected as shown in figure 3. As a consequence, the EC beam is now spread over the graphite tile leading to an elliptical beam pattern on target ($w_x > w_y$).

Similarly to the previous analyses, the pixel size is determined with the CAD drawing which allows plotting temperature profile across the tile. We found spatial resolution of 2.8 mm/pixel and 5.9mm/pixel in the horizontal and vertical directions respectively, those values are higher than computed before because of the tile inclination regarding the field of view.

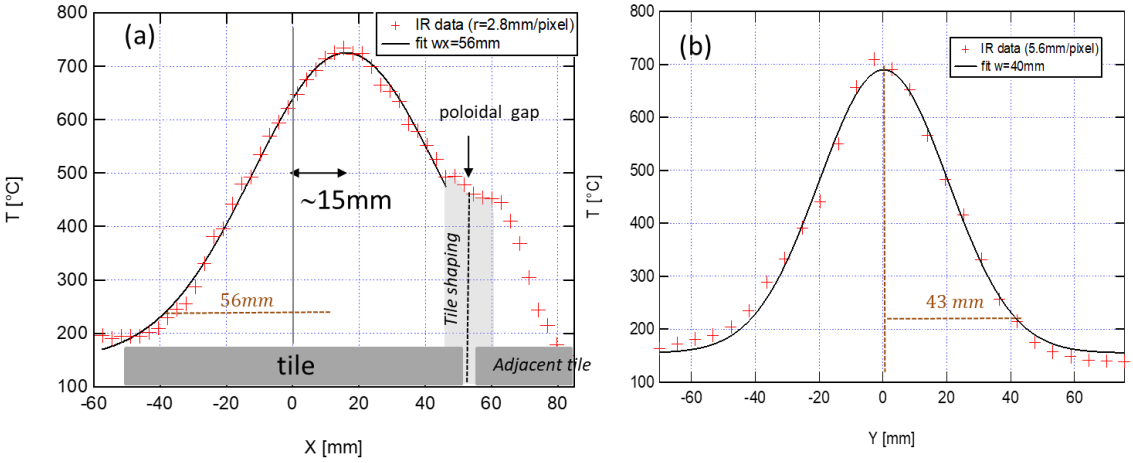


Figure 13: Horizontal (a) and vertical (b) temperature distribution extracted from IR movie at t=8s (#20181009.041, θ=58°, 551 kW continuous). Experimental data are fitted with Gaussian function as given in equation 4. The shaped part of the tile is shown in blue as well as the poloidal gap (limit to the adjacent tile).

Figure 13 shows the temperature distribution profiles along the horizontal and vertical coordinates. The beam size derived from Gaussian fit (equation 4) are $w_x = 56 \pm 2mm$ and $w_y = 43 \pm 2mm$. The horizontal value is almost a factor 1.4 higher than beam size derived at normal incidence and in the vertical direction (w_y~ 43 mm). The beam is shifted by about 15 mm in the X-direction regarding the center of the tile (this is taken into account in the thermal modelling). Thermal modelling is again performed in an iterative way: heat flux absorbed by the graphite (q_n) and thermal resistance (R_c) are adjusted to match the IR measurement during heating and cooling phase respectively. The initial tile temperature is T_0 = 70°C. We found a good match between IR data and modelling assuming ECRH beam shifted by 15mm from the center of the tile with q_n decreasing from 2.86 MW.m^{-2} down to 2.3 MW.m^{-2} at the end of the pulse and $R_c = 2 \times 10^{-4} m^2 K/W$ (see figure 14). A small discrepancy is observed at the beginning of the pulse, this could be explained by parasitic light emitted from the island-divertor or baffle and reflected from the inner-wall, which could be significant when the plasma starts and becomes negligible as the temperature increases.

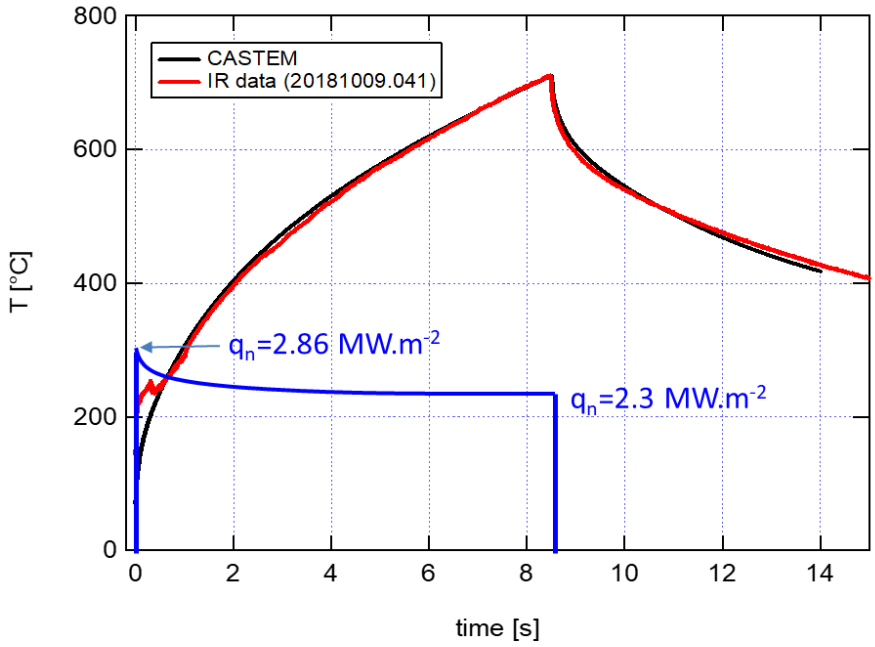


Figure 14: Maximum temperature on tile surface, IR measurement (red line), CASTEM simulation (black line) and maximum heat load (blue line) computed after the iterative loop.

Due to the shallow incidence to the plasma axis, the used O2-mode polarization is nearly circular so that the electric field has equal shares over time in parallel and perpendicular direction to the incidence plane. For this reason, one can assume an averaged absorption of $\eta_C = 0.5 \times \left(\eta_{//} + \eta_{\perp}\right) = 0.5 \times \eta_C(0°) \times \left(\frac{1}{\mathrm{Cos}\,\theta} + \mathrm{Cos}\,\theta\right)$ as shown in equation (1). For θ=58° we found $\eta_C = 1.2 \times \eta_C(0°) = 3.6\%$ at room temperature. The ECRH shine through heat flux is determined with equations 8 assuming temperature dependence with the absorption coefficient set to 3.6% at room temperature (figure 15-a), we found $q_{EC}^{trans}(0) \sim 85\ MW.m^{-2}$ almost constant during the pulse. The ECRH shine through power is then computed with equation 5 assuming asymmetric ECRH beam, $w_x = 56\,mm$ and $w_y = 43\,mm$, in the horizontal and vertical directions respectively. The result is presented in figure 15-b assuming constant (blue) and varying (red) absorption with temperature. We found ~322 kW of EC shine through power which is lower than numerical calculation ~390 kW. The discrepancy is about 18% which is however included in the error bars (15% for the numerical calculation and 10% for the experimental data).

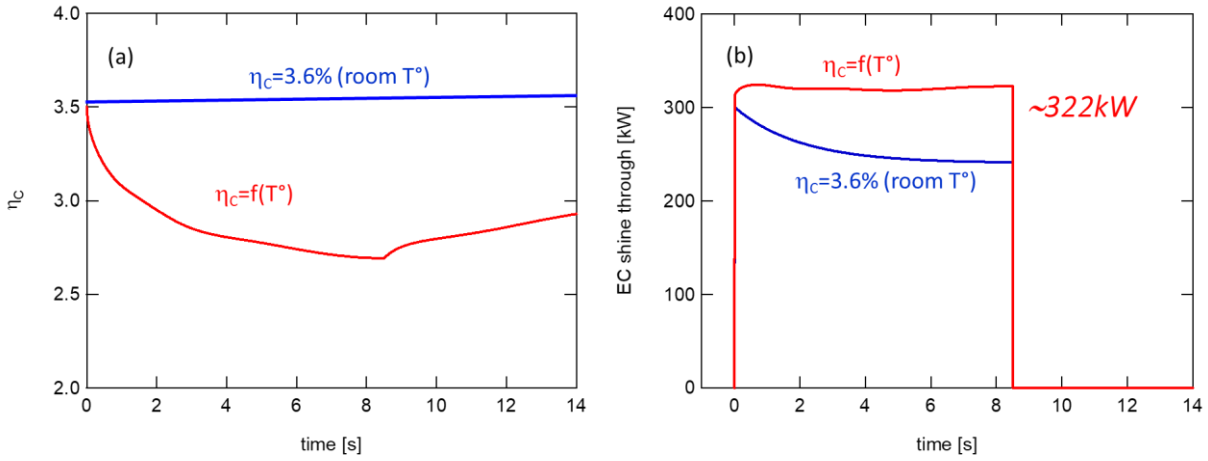


Figure 15: (a) Ohmic absorption computed for each temperature steps. (b) ECRH shine through power estimated as function of time with constant (blue) and non-constant (red) ohmic absorption.

Another physical reason for the discrepancy is the IR temperature measurement which could be more sensitive to optical surface properties because of the inclination of the tile regarding the line of sight (top view). Further experiments with optimized settings (ECRH beam located in the equatorial mid-plane and centered in the IR viewing, cold tile before to start the experiment) would be required to investigate this discrepancy.

6. Conclusion

During a handful of ECRH experiments in OP1.2, an ECRH beam strikes the first wall with different incidence angles, polarizations and intensities. The accordant heat load has been derived using IR thermography measurements on the first wall. The outputs give relevant information regarding two different issues: wall protection and microwave plasma absorption during ECH operation. It shows that IR thermography can be used on top of other protective diagnostics such as stray radiation interlock and RF detectors to directly measure the shine through power. The beam width derived by IR thermography can also be used for the crosscheck of the quasi-optical imaging properties of the ECRH transmission system.

A key parameter to determine the shine through power is the fraction of GHz power losses into the graphite tile (η_C). It has been measured for the first time in-situ, with an empty torus and a beam propagation axis almost normal with the surface (θ=12°). We found power loss fraction of 2.76% in a dedicated experiment without plasma, which is very close to theoretical calculation

assuming perfectly plane surface (2.6%) and laboratory measurement (3% found at room temperature).

The shine through power have been computed using IR data for two different EC beam power (775 kW pulsed and 550 kW steady) and two different angle of incidence, θ=17° and θ=58° respectively. The ratio between the power losses (q_n) with the absorption coefficient (η_C) enables to determine the transmitted power after the first path absorption (q_{EC}^{trans}) whether the absorption coefficient of the particular surface is known. For the pulse with pure O2-mode heating and shallow beam angle analyzed in this paper, the shine through power derived from IR measurements is found to be 58% of the total injected power which is lower with theoretical calculation giving 70%. For the pulse with O/X mixture of polarization and beam angle almost normal to the first wall, the shine through power derived from IR measurements is found to be 58% of the total injected power while theoretical calculation gives only 30%.

The methodology developed and demonstrated in this paper can be useful for the design and development of ECRH protective diagnostics, calibration and operation of the ECRH systems in the next step fusion devices. During the First Plasma Operation Phase of ITER for instance, the ECRH beams will be reflected on copper-coated mirrors located on the inboard side of the tokamak before passing through the plasma to assist plasma breakdown and burn-through [22]. IR imaging is foreseen to monitor the position of the ECRH beams on these mirrors as well as one of the four temporary limiters. A rigorous estimate of the absorption coefficient by the microwaves of the components heated by ECRH, like the first wall, some diagnostic components or ECRH mirrors, will be essential for the IR data analysis during ECRH plasma operation in ITER.

Acknowledgments:
This work has been carried out within the framework of the EUROfusion Consortium and has received funding from the Euratom research and training programme 2014-2018 and 2019-2020 under grant agreement No 633053. The views and opinions expressed herein do not necessarily reflect those of the European Commission

References:

[1] Erckmann, V., Brand, P., Braune, H., Dammertz, G., Gantenbein, G., Kasparek, W., … Weller, A. (2007). Electron Cyclotron Heating for W7-X: Physics and Technology. *Fusion Science and Technology*, *52*(2), 291–312. Retrieved from http://epubs.ans.org/?a=1508

[2] Michel, G., Erckmann, V., Hollmann, F., Jonitz, L., Kasparek, W., Laqua, H., Weißgerber, M. (2013). Matching of the ECRH transmission line of W7-X. *Fusion Engineering and Design*, *88*(6–8), 903–907. https://doi.org/10.1016/J.FUSENGDES.2012.11.026

[3] Preynas, M., Laqua, H. P., Marsen, S., Reintrog, A., Corre, Y., Moncada, V., & Travere, J.-M. (2015). A near infra-red video system as a protective diagnostic for electron cyclotron resonance heating operation in the Wendelstein 7-X stellarator. *Review of Scientific Instruments*, *86*(11), 113504. https://doi.org/10.1063/1.4935686

[4] Moseev, D., Laqua, H. P., Marsen, S., Stange, T., Braune, H., Erckmann, V., Oosterbeek, J. W. (2016). Absolute calibration of sniffer probes on Wendelstein 7-X. *Review of Scientific Instruments*, *87*(8), 83505. https://doi.org/10.1063/1.4960349

[5] Marsen, S., Corre, Y., Laqua, H. P., Moncada, V., Moseev, D., Niemann, H., Team, T. W.-X. (2017). First results from protective ECRH diagnostics for Wendelstein 7-X. *Nuclear Fusion*, *57*(8), 86014. https://doi.org/10.1088/1741-4326/aa6ab2

[6] M. Jakubowski,P. Drewelow, J. Fellinger, A. Puig Sitjes, G. Wurden, A. Ali, C. Biedermann, B. Cannas, D. Chauvin, M. Gamradt, H. Greve, Y. Gao, D. Hathiramani, R. Konig, A. Lorenz, V. Moncada, H. Niemann, T. Thanh Ngo, F. Pisano, T. Sunn Pedersen, and W7-X Team. *Review of Scientific Instruments*, 89, 10E116 (2018) https://doi.org/10.1063/1.5038634

[7] Klinger, T., Baylard, C., Beidler, C. D., Boscary, J., Bosch, H. S., Dinklage, A., Wolf, R. (2013). Towards assembly completion and preparation of experimental campaigns of Wendelstein 7-X in the perspective of a path to a stellarator fusion power plant. *Fusion Engineering and Design*, *88*(6–8), 461–465. https://doi.org/10.1016/J.FUSENGDES.2013.02.153

[8] Ray-tracing code TRAVIS for ECR heating, EC current drive and ECE diagnostic N.B. Marushchenko, Y. Turkin, H. Maassberg. Computer Physics Communication. Volume 185, Issue 1, January 2014, Pages 165-176. http://dx.doi.org/10.1016/j.cpc.2013.09.002

[9] Klinger T, et al. (2019) Overview of first Wendelstein 7-X high-performance operation, *Nucl. Fusion 59*. https://doi.org/10.1088/1741-4326/ab03a7

[10] Measurements of ohmic losses of metallic reflectors at 140 GHz using a 3-mirror resonator technique. W. Kasparek, A. Fernandez, F. Hollmann and R. Wacker. International Journal of Infrared and Millimeter waves. Vol. 22. N°11, November 2001.

[11] Gaussian Beam Quasioptical Propagation and Applications. P. Goldsmith. Wiley Publisher (microwave theory and techniques society). IEEE press

[12] "Three-mirror resonator reflectivity measurement of plane and grooved surfaces: Setup, options, results" W. Kasparek et al., 2012 6th European Conference on Antennas and Propagation (EUCAP), Prague, 2012, pp. 585-589, doi: 10.1109/EuCAP.2012.6206543.

[13] C. Ruset et al. Fusion Engineering and Design 86 (2011) 1677–1680

[14] Mendelevitch B., Vorköper A., Boscary J., Li Ch., Dekorsy N., Peacock A., Sellmeier O., Stadler R., Tittes, H, Lessons learned from the design and fabrication of the baffles and heat shields of Wendelstein 7-X, Fusion Engineering and Design 88 (2013) 1660– 1663 http://dx.doi.org/10.1016/j.fusengdes.2013.05.110

[15] Verpaux P., Millard A., Hoffman A. and Ebersolt L. 1988 CASTEM 2000: a Modern Approach of Computerized Structural Analysis (Risley, UK) http://www-cast3m.cea.fr

[16] Wendelstein 7-X Near Real-Time Image Diagnostic System for Plasma-Facing Components Protection. A. Puig Sitjes, M. Jakubowski, A. Ali, P. Drewelow, V. Moncada, F. Pisano, T. T.Ngo, B. Cannas, J. M. Travère, G. Kocsis, T. Szepesi, T. Szabolics & W7-X Team. FUSION SCIENCE AND TECHNOLOGY · VOLUME 74 · JULY–AUGUST 2018. https://doi.org/10.1080/15361055.2017.1396860

[17] Initial results from the hotspot detection scheme for protection of plasma facing components in Wendelstein 7-X. A. Ali, H. Niemann, M. Jakubowski, T. Sunn Pedersen, R. Neu, Y. Corre, P. Drewelow, Puig Sitjes, G. Wurden, F. Pisano, B. Cannas, Y. Gao, M. Ślęczka and the W7-X Team Nuclear Materials and Energy 19 (2019) 335–339. https://doi.org/10.1016/j.nme.2019.03.006

[18] Limiter observation during W7-X first plasmas. G.A. Wurden, C. Biedermann, F. Effenberg, M. Jakubowski, H. Niemann, L. Stephey, S. Bozhenkov, S. Brezinsek, J. Fellinger, B. Cannas, F. Pisano, S. Marsen, H.P. Laqua, R. König, O. Schmitz, J.H. Harris, E.A. Unterberg and the W7-X Team. Nucl. Fusion 57 (2017) 056036 (11p)

[19] H. Laqua et al. "Overview of W7-X ECRH Results in OP1.2a". EPJ web conference. Volume 187, 01011 (2018). 30th Joint Russian-German Meeting on ECRH and Gyrotrons. https://doi.org/10.1051/epjconf/201818701011

[20] V. MARTIN et al., "Integrated Software for Imaging Data Analysis Applied to Edge Plasma Physic and Operational
Safety," Fusion Eng. Des., 86, 270 (2011);
https://doi.org/10.1016/j.fusengdes.2010.10.004

[21] Towards a new image processing system at Wendelstein 7-X: From spatial calibration to characterization of thermal events. F. Pisano, B. Cannas, M. Jakubowski, H. Niemann, A. Puig Sitjes, G.A. Wurden and W7X team. Rev. Sci. Instrum. 89, 123503 (2018). https://doi.org/10.1063/1.5045560

[22] M.A. Henderson et al. « EU developments of the ITER ECRH system". Fusion Engineering and Design 82 (2007). https: doi:10.1016/j.fusengdes.2007.01.029